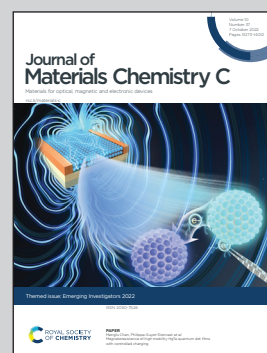**Showcasing research from Professor Xiao Li's laboratory, Materials Science and Engineering, University of North Texas, Denton, USA.**

Synergistic self-assembly of rod-like monomers in blue phase liquid crystals for tunable optical properties

The polymerization of 3D cubic structures assembled from blue phase (BP) liquid crystals has been recognized for the remarkable properties displayed after a fluid structure is transformed into a template. Selective reflection of visible light and fast response time are the key characteristics that influence the application in photonic crystals, displays and actuators. Here, based on mixing of rod-like mesogenic monomers in BP lattices, the synergistic self-assembly behaviour of the monomers and the effect of monomer composition and concentration on BP lattice are revealed during soft crystal growth and transformations, providing tunable optical properties.

As featured in:

See Xiao Li *et al.*,
J. Mater. Chem. C, 2022, **10**, 13778.

ROYAL SOCIETY OF CHEMISTRY

rsc.li/materials-c

Journal of Materials Chemistry C

Synergistic self-assembly of rod-like monomers in blue phase liquid crystals for tunable optical properties†

Tejal Pawale, [a] Savannah Cheng,[ab] Nataliia Hnatchuk[a] and Xiao Li *[a]

The three-dimensional nanostructures of blue phase liquid crystals (BPLCs) are becoming the spotlight of soft matter research in electro-optic devices, sensors, photonic crystals, and 3D lasers. The polymerization of the blue phase system overcomes the inherent thermal instability and paves the way for broadening the application of blue phases. Prior to polymerization, a fundamental understanding of the synergistic self-assembly behavior of monomers in the BP lattice can provide insights not only into the soft crystal growth and crystal transformations but also into the tunability of their optical properties. Here, we controlled the reactive monomer content in the BPs to observe the stability of BPI and BPII with different lattice dimensions before polymerization. The self-assembly behavior of commercially available rod-like mesogenic monomers in BP lattices with different monomer compositions was investigated under a homogeneous hybrid cell and directed self-assembly approach. The revealed synergistic self-assembly mechanism of the mesogenic monomer in BPs provides the ability to tune the photonic band gap of BP soft crystals.

[a] *Department of Materials Science and Engineering, University of North Texas, 3940 N. Elm, Denton, TX 76207, USA. E-mail: Xiao.Li@unt.edu*

[b] *Texas Academy of Mathematics & Science, University of North Texas, 1155 Union Circle #305309, Denton, TX 76203, USA*

† Electronic supplementary information (ESI) available. See DOI: https://doi.org/10.1039/d2tc01333a

Xiao Li *is an assistant professor in the Department of Materials Science and Engineering, University of North Texas. She received her PhD in Polymer Chemistry and Physics from Changchun Institute of Applied Chemistry, Chinese Academy of Sciences. She did postdoctoral research in Chemical & Biological Engineering at the University of Wisconsin-Madison (2012–2013), and Pritzker School of Molecular Engineering at the University of Chicago (2013–2015). She was also a research scientist at the University of Chicago (2015–2019), and a visiting resident associate at Argonne National Laboratory (2015–2019). Her current research interests focus on the self-assembly of block copolymer, liquid crystals, colloidal particles and liquid crystal elastomers for optoelectronic, biomedical and microactuator applications.*

Xiao Li

Introduction

The fluid lattice structure of blue phases (BPs) stabilized by lattice defects has been a subject of considerable interest over the last few years given the spontaneous formation of 3D cubic symmetries. The unique nature of BPs is based on the packing topology and the chiral force interrelation. In BPs, the molecules adapt the configuration to experience double-twisting along the *x*- and *y*-axes, resulting in double-twist cylinders (DTC). Moreover, disclination lines are generated to fill the unoccupied space and stabilize the three-dimensional cubic morphology formed by DTC. Three types of BP crystal structures are observed, namely BPI, BPII, and BPIII, depending on the thermodynamic conditions. The structure of BPI is body-centered cubic, BPII is simple cubic, and BPIII is amorphous in nature.[1] For both cubic symmetries, the BP lattice parameters are of the order of hundreds of nanometers, leading to the Bragg reflection of visible light, which is desirable in electro-optic devices,[2] photonic crystals[3–5] and displays. However, the grain boundaries of the multi-platelet domains hinder the applicability of BP in such devices. So far, different techniques have been implemented, such as external stimuli,[6–8] thermal treatment,[4] or surface treatments,[9,10] to facilitate the formation of monodomains or single-crystals of BPs. In particular, the chemically patterned surfaces with regions of different anchoring strengths enabled the nucleation and growth of arbitrary large BP single-crystals.[9,10] Although the coexistence of DTC

and disclination lines generates a stable structure, it also restricts the BP appearance to a narrow temperature range due to the competition between the local energetic minimization of DTC and the defects of instabilities in the global structure, thus limiting the practical applications. Numerous strategies have been implemented to design BPLC systems to stabilize BPs over a wider temperature range, including the synthesis of liquid crystal molecules with fluoride atoms,[11] and the introduction of low-weight molecules,[12–19] nanoparticles,[20,21] and polymers[22] into the system. The most conventional method for maintaining the cubic lattice structure is to polymerize reactive monomers within the BPLC yielding a temperature range greater than 60 K.[23] It is speculated that the polymer chains grow along the disclination lines after photopolymerization to stabilize the core of the BPLC structure, thus causing the expansion of the temperature range.[24] Employing monomers with different compositions, shapes, and functional groups affects the thermal stabilization capabilities of the formed blue phases *via* polymerization. So far, numerous BP-monomer systems have been developed to achieve wider temperature range stability, for instance, rod-like monomers, flexible side-chain monomers,[25] bent-shaped monomers,[12,13,19] chiral dopants with reactive acrylate groups[26] and hydrogen bond formation.[16] This further enables the additional functionalities, such as photonic bandgap tunability[27] and the stimuli-responsive behavior of BP elastomers.[28,29] Another promising way to stabilize the BPs involves the inclusion of low molecular weight LC molecules such as LC dimers,[11] W-shaped,[14] bent and T-shaped H-bonded molecules,[15,17] banana shaped,[30] *etc.* The importance of the synergistic self-assembly of LC molecules/mesogen in controlling the thermal stability of the system is revealed by using multi-component BPs of uniaxial rod-like and biaxial dimers.[11] The fundamental understanding of additive molecular diffusion and self-assembly in BP lattices, especially the evolution of cubic structure caused by phase transitions, is particularly important in both cases. However, since most research is focused on increasing the thermal appearance of the blue phase using polymerization, limited studies have investigated the effect of active monomer self-assembly on the BP lattice.

The main purpose of this work is to elucidate the relationship between the molecular self-assembly of conventional rod-like reactive monomers in the BP lattice and the tunability of BP optical properties. In order to understand the self-assembly mechanism of reactive monomers (RMs) in the BP lattice, we investigated the lattice orientation and lattice parameter changes of the blue phase system after the addition of RMs. The rationale is that the configurational similarity of the mesogenic core between RM and LC molecules enables the synergistic self-assembly into DTC. Such behavior not only enhances thermal stability prior to polymerization but also affects the orientation and lattice parameters of BPs. From direct optical characterization, we observe the phase transition and lattice parameter changes leading to the variation in reflective color. The addition of rod-like monomers with relatively different flexibility enlarged the lattice of BPII (100) from

155 nm to 179 nm by a shift in reflection color from blue to green. For BPI (110) the lattice size changed from 240 nm to 285 nm with the transition from green to a red domain. Thus, depending on the similar mesogenic core configuration of RM introduced into BP, the system offers the ability to tune the optical properties of BP. We anticipate that the revealed synergistic self-assembly mechanism of mesogenic monomer will provide tunability of the BP 3D structure prior to polymerization, facilitate the new design of reactive monomers, and enable applications in photonics without any external stimulus, depending only on the composition and concentration of the RM.
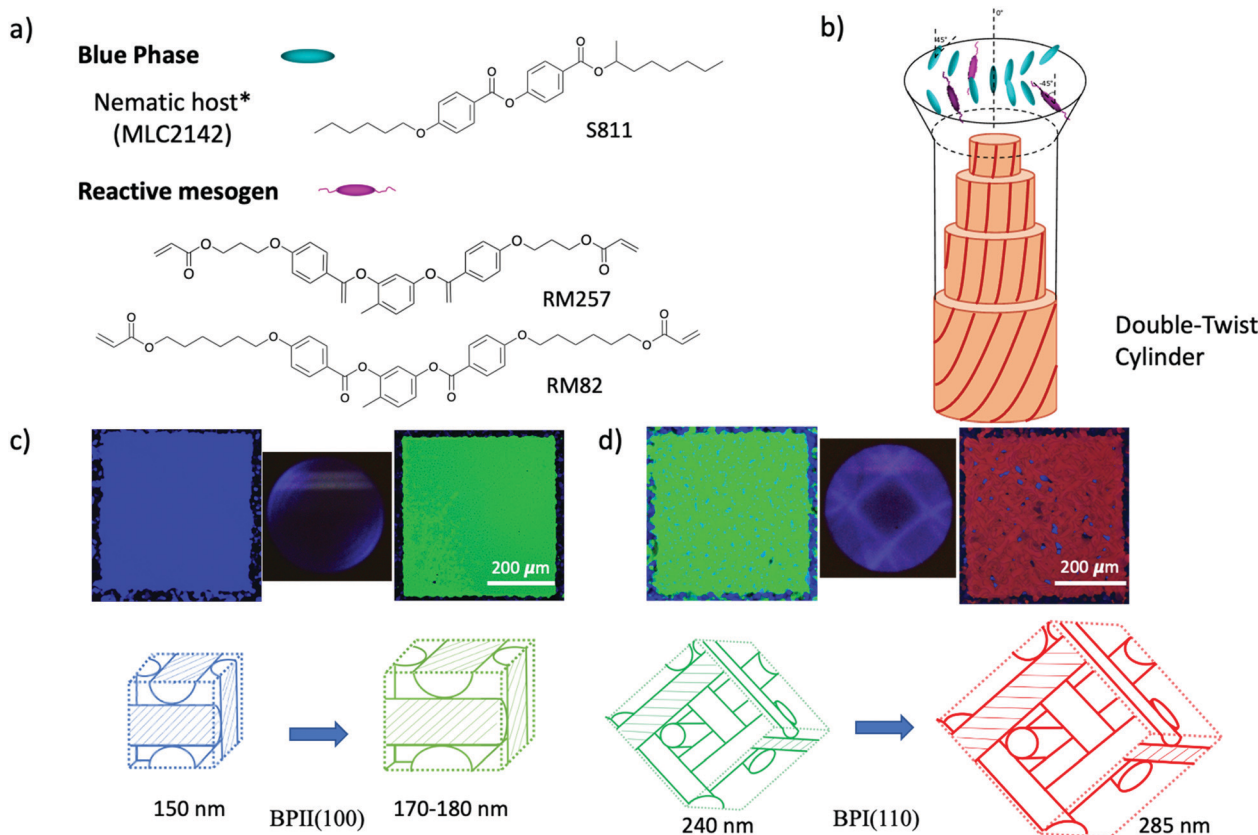
Results

Unlike previously reported studies that polymerized reactive monomers and cross-linkers to thermally stabilize the blue phase, herein, we focus on investigating the self-assembly of rod-like monomers within the BP crystal lattice before polymerization. The chiral dopant S811 was mixed in nematic liquid crystal MLC2142 at the concentration of 36.32 wt% to prepare the blue phase of the liquid crystal. The prepared BP mixture was blended with monomers of different compositions and weight fractions. Chemical structures of the compounds used for this study are presented in Fig. 1a, including the reactive mesogen of 1,4-phenylene bis(4-(6-(acryloyloxy)hexyloxy)benzoate) (RM82), (1,4-bis-[4-(3-acryloyloxypropyloxy)benzoyloxy]-2 methylbenzene (RM257), non-mesogenic monomer of trimethylpropane triacrylate (TMPTA) and photoinitiator 2,2-dimethoxy-2-phenylacetophenone (Irg651). A non-mesogenic monomer and photoinitiator were added to the mixtures of BP and RMs; the system was then further analyzed before and after UV polymerization. The solution was confined in a 3.5 μm thick liquid crystal cell consisting of an octadecyltrichlorosilane (OTS)-coated glass top surface and the silicon bottom surface (substrate). The mixtures were injected into the liquid crystal cell above the isotropic temperature *via* capillary force. The self-assembly of the monomer in the blue phase lattice was observed on the silicon substrate with different anchoring conditions: planar anchoring and the chemical pattern of alternating planar and homeotropic anchoring stripes with a 150 nm period, which has been reported to direct BP single-crystal self-assembly.[9,10] The 3D nanostructure of the BP lattice allows the efficient study of the BPLC system using Bragg diffraction-based experimental methods, such as Kossel pattern and reflectance spectroscopy. According to Braggs law, the (*hkl*) planes of a lattice correspond to the selective reflection wavelength:

$$\lambda_{(hkl)} = 2na \left/ \sqrt{h^2 + k^2 + l^2} \right. \tag{1}$$

where n is the refractive index of the medium, a is the lattice size and (*hkl*) are Miller indices. Utilizing the convergent monochromatic light, the diffraction patterns can be obtained for the BP cubic structure, which provides information on the specific lattice orientation (*i.e.*, *hkl*). Thus, combining the lattice orientation and reflection wavelength for different RM added to BP systems during thermal cycling enables the study of the BP crystal evolution. The

This journal is © The Royal Society of Chemistry 2022

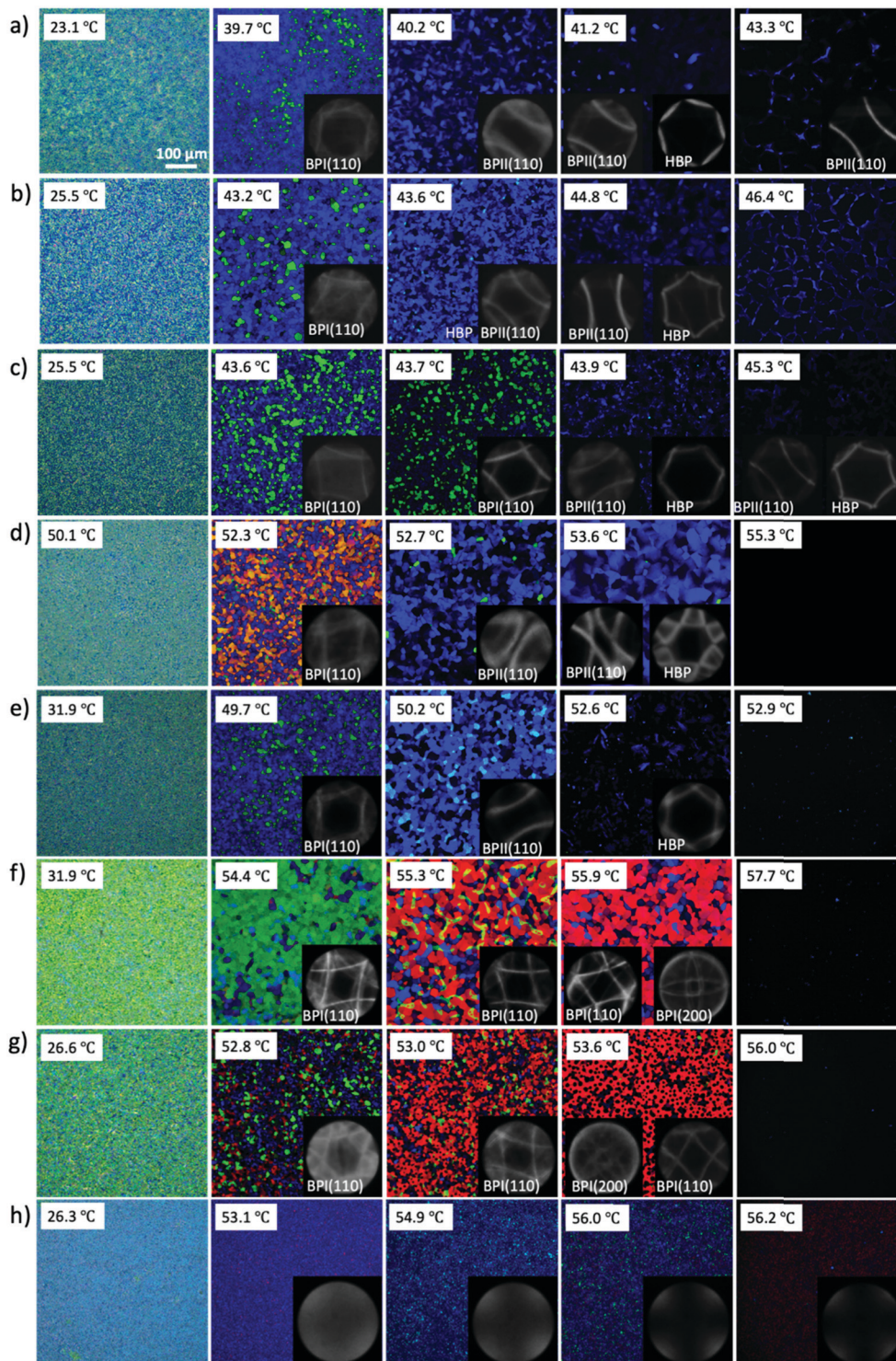*J. Mater. Chem. C*, 2022, **10**, 13778–13788 | **13779**

Fig. 1 (a) Chemical formulae of the chiral dopant and RMs. (b) Schematic of the molecules' self-assembly in the double-twist cylinders. POM images of the (c) BPII (100) and (d) BPI (110) orientation as a function of reflection wavelength and lattice size. Scale bar: 200 μm.

conventional rod-like monomers (RM) have a similar mesogenic core configuration to the host LC molecules and arrange themselves along with LC molecules in DTC. Fig. 1b represents the self-assembly of RM along with LC molecules forming double-twist cylinders, thereby causing the change in the lattice parameters of the generated blue phase. Fig. 1c and d illustrate the change in the reflected color when the BP lattice undergoes a dimensional change. For BPII (100) (Fig. 1c), the transition from blue to green indicates the increase in lattice size, while for the BPI (110) orientation (Fig. 1d), a similar trend is observed when the reflected color changes from green to red.

In order to understand the self-assembly behavior of reactive mesogens in the blue phase system, firstly reactive mesogen RM82 with different concentrations was introduced into the blue phase. A hybrid liquid crystal cell with a planar anchored bottom and homeotropic (OTS-modified) top substrate was used to characterize the changes in the lattice orientation and parameters. Fig. 2 presents polarized optical microscopy (POM) images of the BP morphologies and the corresponding diffraction pattern of Kossel diagrams for the heating cycle from the cholesteric (Chol) to isotropic (Iso) phase at the rate of 0.1 °C min^{-1}. For the pure BP mixture, the phase transition was observed as Chol–BPI at 41.0 °C, BPI–BPII at 42.0 °C and BPII–Iso at 44.0 °C. Table 1 summarizes the different tested compositions and transition temperature ranges in hybrid

anchored cells. The phase transition temperature of BP/RM82 solutions for hybrid confinement (S1-a) and DSA (S1-b) are provided in Fig. S1 (ESI†). When the RM concentration is higher than 13.0 wt% in the hybrid confinement and 9.6 wt% in the case of DSA, the addition of RM results in a retardation of the phase transition temperature of the blue phase and also inhibits BPII. The concentration of added monomer was gradually increased from 4.0 wt% (Fig. 2a) to 20.0 wt% (Fig. 2h). Adding RM82 to the concentrations from 4.0 wt% to 13.0 wt% narrowed the temperature range for BPI while extending it for BPII. In the case of BPI, the two-fold symmetry of the Kossel pattern indicated the (110) orientation.[31] The undefined Kossel lines represent the non-uniform formation of BPLC on the surface. On the other hand, for BPII, the two curves signal the (110) orientation and the hexagonal pattern corresponds to the hexagonal blue phase (HBP).[7] The shift in the reflective color from BPI to the isotropic phase for different RM82 weight fractions was recorded with respect to the temperature by using an optical spectrometer (Fig. 3). The wavelength transition with increasing temperature was due to the phase transition from BPI to BPII. In contrast to the concentrations below 13.0 wt%, for 15.0 and 17.0 wt%, only BPI was formed from the cholesteric to the isotropic phase. The temperature span of BPI was extended to ∼3.2 °C from the previous ∼1 °C range. At 15.0 wt% RM82, the Kossel lines demonstrated BPI with the

13780 | *J. Mater. Chem. C*, 2022, **10**, 13778–13788

This journal is © The Royal Society of Chemistry 2022

Fig. 2 Hybrid confinement of different RM82 concentrations in the BP premixture: (a) 4.0 wt%, (b) 5.6 wt% (c) 7.6 wt%, (d) 9.6 wt%, (e) 13.0 wt%, (f) 15.0 wt%, (g) 17.0 wt%, (h) 20.0 wt%. Scale bar: 100 μm.

(110) orientation and distortion of the BPLC along the (001) axis led to the tetragonal symmetry at 54.4 °C.[32] As the temperature increased, the green color reflected by BPI (110) transitioned to red and the Kossel lines of BPI turned by ∼90° with respect to the [001] crystal axis of the BP lattice.[33] A further increase in temperature led to the polycrystalline nature of BPI with the (200) lattice orientation accompanying BPI (110). The changes in the reflection color indicated the shift in the wavelength from 440 nm to 600 nm in both cases (Fig. 3). The domain size of the BPI crystal generated at 17.0 wt% was smaller than at

This journal is © The Royal Society of Chemistry 2022

J. Mater. Chem. C, 2022, 10, 13778–13788 | 13781

Table 1 The temperature ranges of BP phases for RM mixtures under hybrid cell confinement

Sample no	RM257 (wt%)	RM82 (wt%)	BPI (°C)	BPII (°C)	ΔT (°C)
1	4.0	0	0.4	3.0	3.4
2	5.6	0	0.3	2.7	3.0
3	7.6	0	1.2	2.4	3.6
4	9.6	0	2.8	—	2.8
5	13.0	0	—	—	—
6	0	4.0	0.9	3.0	4.2
7	0	5.6	0.4	3.2	3.6
8	0	7.6	0.3	2.9	3.1
9	0	9.6	0.4	2.6	3.0
10	0	13.0	0.5	2.7	3.2
11	0	15.0	3.3	—	3.3
12	0	17.0	3.2	—	3.2
13	0	20.0	—	—	—
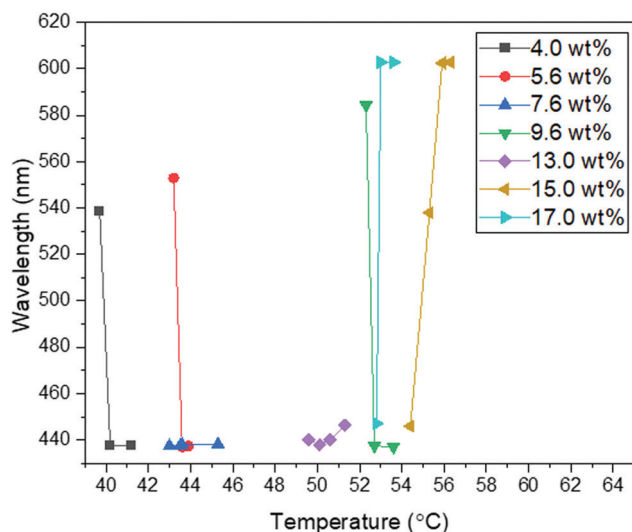
Fig. 3 The relative wavelength *vs.* temperature for RM82 weight fractions in hybrid cell confinement.

15.0 wt% of RM82. The formation of black microdomains and their expansion were observed closer to the isotropic temperature. Eventually, when the monomer concentration reached 20.0 wt%, the BP system failed to assemble into domains recognizable by the Kossel patterns.

The confinement of the BP/RM82 mixture in hybrid anchored cells provides insight into the BP behavior *via* Kossel diagrams and spectrophotometer data when RM is present in the system. The obvious BPII stabilization with narrowed BPI temperature range for weight fractions below 13.0 wt% remained to be analyzed due to the polycrystalline nature of BP. The inability to grow larger domains of the blue phase without an external treatment prohibited further examination of the RM assembly in the BP lattice. To eliminate the grain boundaries and investigate the system on the BP single-crystal, a directed self-assembly approach was employed.[9] From previous studies, a nanopatterned substrate with alternate regions of planar and homeotropic anchoring can promote the nucleation of BP single-crystals with the preferred lattice orientation depending on the period and width of the pattern regions. Thus, a chemical pattern with a 150 nm period and 75 nm planar anchored stripe width was utilized in this research, resulting in the growth of BPII single-crystals with (100) orientation.[10] BP single-crystals engineered to favor an orientation provide a straightforward approach to investigating the effect of reactive mesogens on the changes in the BP lattice.

Following a similar experimental procedure to the hybrid anchored cell, the various monomer concentrations and the thermal transition from the Chol–Iso phase were studied for the chemically patterned substrate. Fig. 4 displays the POM images and Kossel diagrams of RM82 from 0.0 wt% (Fig. 4a) to 20.0 wt% (Fig. 4h) as the sample was heated from the Chol–Iso phase. In the case of pure BP, initially, at the Chol–BPI transition temperature, platelets of BPI (110) were generated over the pattern region. Finally, at the BPI–BPII transformation, a single crystal of BPII (100) occupied the entire pattern area, which was confirmed by the Kossel diagram. According to the samples tested in the hybrid confinement, above 5.6 wt% and below 13.0 wt% RM82, the BPI was suppressed to the narrow temperature range of <0.5 °C, which is aligned with 5.6–9.6 wt% RM82 in the pattern area. The two-fold symmetry of Kossel lines in each case represents the lattice orientation of (110) with similar directions of easy axes [100]. The nucleation of the BPII single-crystal at the BPI–BPII transition was instant and the Kossel diagrams representing (100) orientation remained until the clearing point. Moreover, 7.6 wt% RM82 (Fig. 4c) showed a prominent color change from the initial blue BPII single-crystals to green with the rising temperature. The transformation of BPII reflective colors with temperature variation indicated that the photonic band gap (PBG) shifted from 465 nm to 510 nm for 5.6 wt%, and from 487 nm to 511 nm for 7.6 wt%, respectively, as shown in Fig. 5. However, the reflective wavelength of BPI and BPII matched for 9.6 wt% RM82, and the Kossel lines with four arcs represent the BPI (110) orientation at 42.8 °C, which changed to BPII (100) at 43.0 °C. Further heating led to the formation and growth of black microdomains over the pattern region closer to the isotropic phase while maintaining an increase in wavelength. In each case, with the increase in temperature, the single-crystals of BPII (100) transformed into the BP monodomain as clearly seen in the POM images (Fig. 4b and c). The diffraction pattern of Kossel diagrams retained the identical line features over the entire tested BPII temperature range, proving the monodomain crystal nature. Contrary to the hybrid confinement, 13.0 wt% RM82 on the chemically patterned surface only stabilized BPI for the entire temperature range. The reflective wavelength for BPI remained at 510 nm from 53.4 °C to 54.0 °C and shifted to 525 nm at 54.5 °C. Above 13.0 wt% RM82 the systems behaved similarly to the hybrid confinement with the thermally induced transition in reflective color for the BPI lattice with (110) orientation. The deformation of the crystal along the [001] direction transformed the cubic BPI into the tetragonal symmetry.[34] For 15.0 and 17.0 wt% RM82, initially the BPI formed a monodomain crystal over the patterned region and at higher temperatures, small domains of different colors were
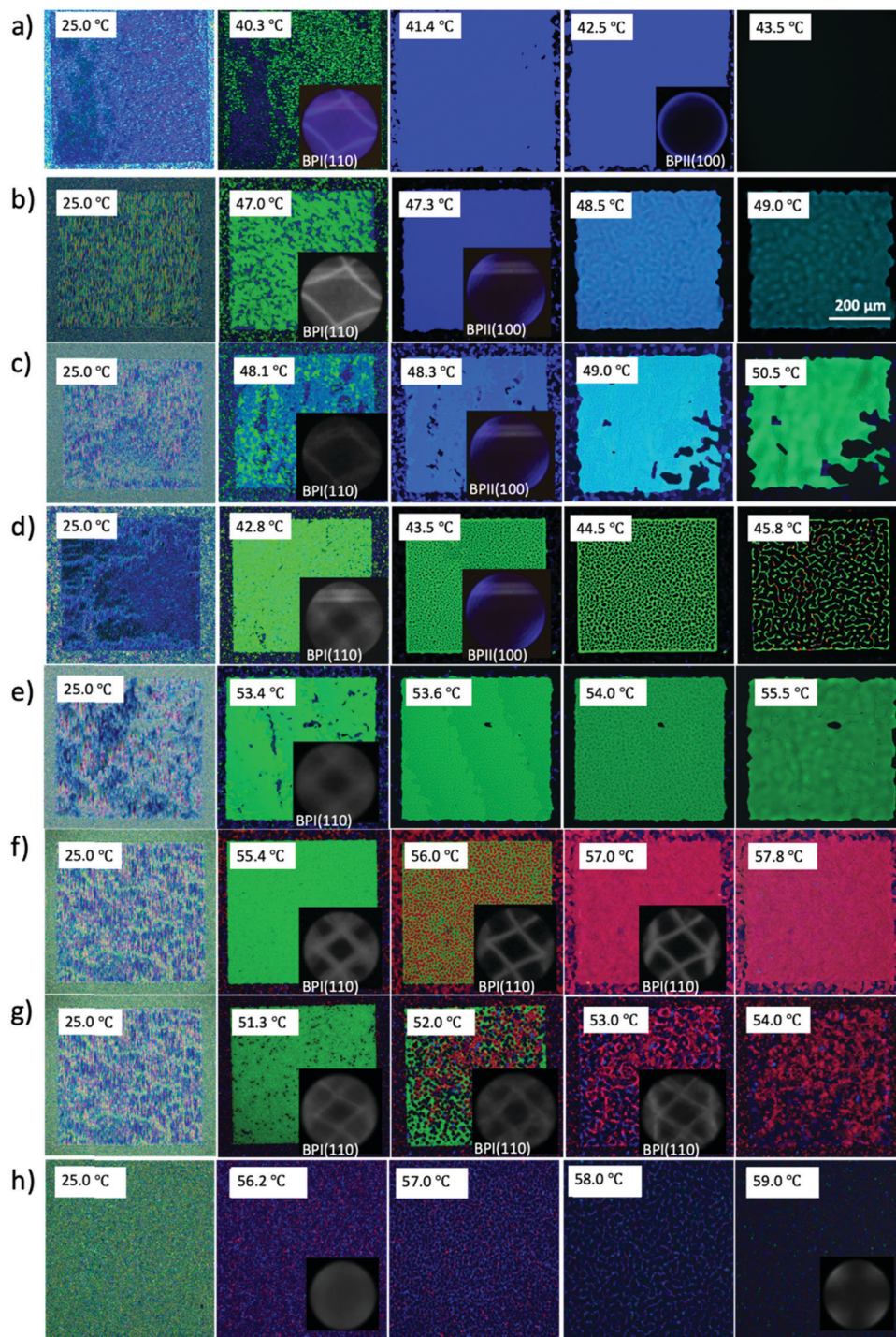
13782 | *J. Mater. Chem. C*, 2022, **10**, 13778–13788

This journal is © The Royal Society of Chemistry 2022

Fig. 4 POM images of RM82 on chemically patterned substrates with concentrations of (a) 0.0 wt%, (b) 5.6 wt%, (c) 7.6 wt%, (d) 9.6 wt%, (e) 13.0 wt%, (f) 15.0 wt%, (g) 17.0 wt%, and (h) 20.0 wt%. Scale bar: 200 μm.

nucleated and further grew over the entire area. The addition of 17.0 wt% RM82 induced a larger domain size in comparison to the 15.0 wt% system. The formed microdomains occupied the entire pattern region at 57.0 °C for 15.0 wt% RM82, whereas 17.0 wt% did not assemble the BP over the whole area. The weak scattered Kossel lines correspond to the inhomogeneous lattice spacing that was eliminated with increasing temperatures. The trend in the shift of the relative wavelength with respect to temperature was similar for both 15.0 and 17.0 wt% RM82, although a larger shift in wavelength of over 79 nm was demonstrated by adding 15 wt% when compared to 65 nm for 17.0 wt% RM82. The directed self-assembly of 20.0 wt% RM82, consistent with the hybrid confinement, was ineffective in nucleating BP crystals on the patterned region.
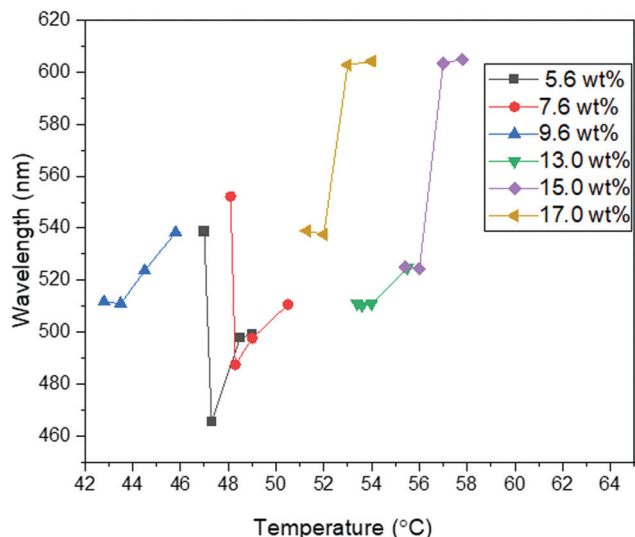
Fig. 5 The wavelength of intensity peaks *vs.* temperature for different concentrations of RM82 in directed self-assembly.

This confirmed that the loss of chirality when the monomer concentration reached 20.0 wt% in the BP premixture led to the failure of the BP assembly.

From the confinement on chemically patterned cells, the self-assembly of RM in the BP lattice can be divided into two regimes depending on the shift in the reflection wavelength and BP states. In the first regime, below 9.6 wt% RM82, the thermal stability of BPII was broadened while the BPI range was narrowed. Additionally, the BPII (100) PBG shift from 460 nm to 510 nm was noted. For the second region with RM above 13.0 wt%, only BPI was stabilized. A large shift in the relative wavelength from 510 nm to 603 nm for BPI (110) tetragonal symmetry was observed.

The non-mesogen monomer TMPTA was added to the solution of BP and 9.6 wt% RM82 to study the synergistic self-assembly of mesogenic and non-mesogenic monomers to thermally stabilize BPLC. TMPTA and photo initiator (Irg651) were doped into the BP premixture together with RM82 as RM82/TMPTA/Irg651:9.3/2.7/0.38 wt%. Prior to polymerization, BPI (110) was generated at 27.5 °C and maintained for a temperature window of 12.0 °C (Fig. 6a). The corresponding Kossel diagrams with two-fold symmetry and the curves indicate the orthorhombic symmetry of BPI (110) orientation. The movement of Kossel lines with increasing temperature pointed to the relaxation of the lattice. As shown in Fig. 6b, with increasing temperature, the reflection wavelength shifted from 524 nm to 584 nm. As a result of the presence of the non-mesogenic monomer, the formation of monodomain BPI (110) was observed instead of single crystals for only RM82. According to our hypothesis, the instability of single-crystal nucleation introduced by the non-mesogen monomer can be related to the accumulation of TMPTA along the disclination lines. During polymerization, the mesogenic monomer was positioned in the twisted cylinders and shifted to make contact with TMPTA in the disclination lines. The synergistic self-assembly of TMPTA

and RM82 reinforces the BP cubic structure *via* the template of the BPI disclination line network. At 29.2 °C, the BPI (110) was polymerized with 2% intensity for 2 minutes. After polymerization, the intensity peak shifted from 551 nm to 535 nm, and the resulting BPI maintained its stability over the temperature range of 100.0 °C.

To further verify the monomer contribution to the BP assembly, we introduced RM257 into the BP mixture instead of RM82, following the same experimental procedure. RM257 has an identical mesogenic core to RM82, but relatively few carbons at the two ends, reducing the molecular flexibility. Based on the obtained results provided in the supporting information, the BPII was stabilized until 7.6 wt% RM257, while BPI was in the 9.6–13.0 wt% range (Fig. S2, ESI†). Above 13.0 wt%, neither BPI nor BPII phases were generated. For the directed self-assembly approach, the transition behaviors of BPII and BPI matched RM82, however, the concentrations shifted towards the lower values (Fig. S3, ESI†). The Kossel diagrams for BPI showed two-fold symmetry with 6 lines indicating the (110) lattice orientation with two easy axis directions.[35] According to the spectrometer data, the relative wavelength moved from 446 nm to 511 nm for BPII (100), whereas for BPI (110) the shift was recorded from 510 nm to 602 nm (Fig. S4, ESI†). The polymerization of the BP cubic structure using RM257 instead of RM82 stabilized the BPI phase in a similar manner (Fig. S5, ESI†). The rigidity of RM257 limited the thermal stabilization ability of the system above 13.0 wt%. The additional chiral dopant S811 was introduced to confirm that the loss of chirality was the reason for BP assembly failure (Fig. 7). As shown in Fig. 7a, the hybrid confinement generated the stable hexagonal blue phase over the temperature span of 3.6 °C. However, for the patterned substrate, only BPI (110) was observed with a transition in reflective color from blue to green (Fig. 7b).

Discussion

In this work, we confirmed the self-assembly mechanism of the rod-like monomers in the double-twist cylinders of the blue phase. The influence of reactive monomers on BP crystal structure formation was investigated under different anchoring conditions. Based on the hybrid confinement, a smaller amount of monomer (below 13.0 wt% for RM82 and 7.6 wt% for RM257) narrowed the temperature span of BPI and stabilized BPII. Free-energy minimization to nucleate BPII (100) single-crystals *via* the designed anchoring conditions assisted the further investigation. The BPII single-crystal along with stabilization showed the variation in the reflective wavelength. This corresponds to the lattice enlargement while approaching the isotropic temperature. Table 2 (RM82) and Table S1 (ESI†) (RM257) summarize the variation in the lattice parameters for the specific lattice orientation as a function of temperature. Above 7.6 wt% RM257 and 13.0 wt% RM82, the BPII was completely suppressed and only BPI remained. The BPI (110) color transition from green to orange to red indicated an
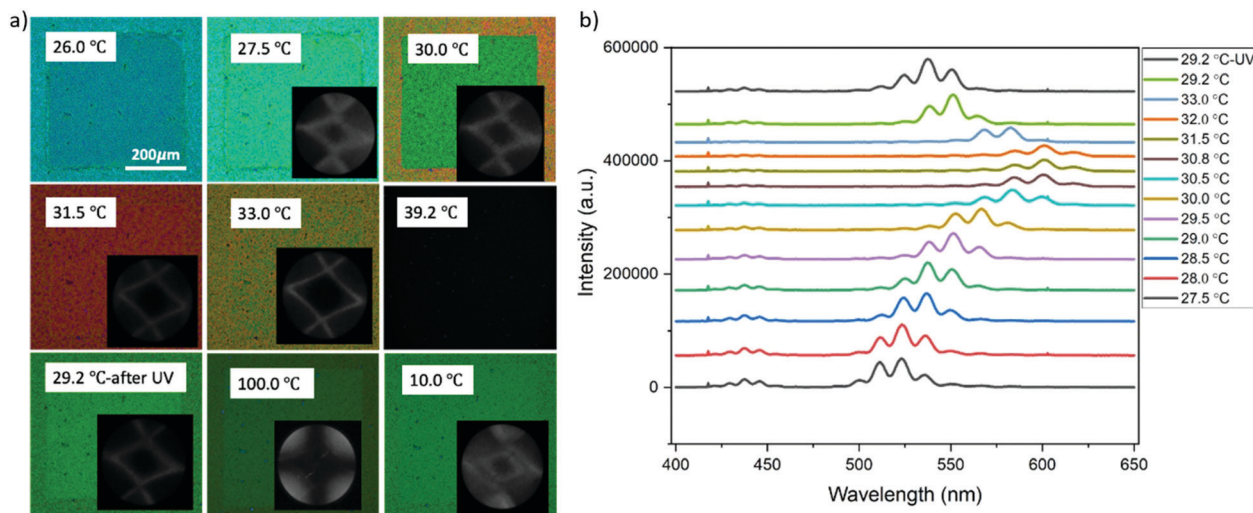
Fig. 6 Polymer stabilization of BPLC on the chemically patterned substrate: (a) POM images of the sample's (RM82/TMPTA/Irg651: 9.3/2.7/0.38 wt%) thermal cycle before polymerization, and BPLC thermal stability after polymerization. Scale bar: 200 μm. (b) The correlation between the wavelength and intensity of RM82/TMPTA/Irg651: 9.3/2.7/0.38 wt% as a function of temperature.
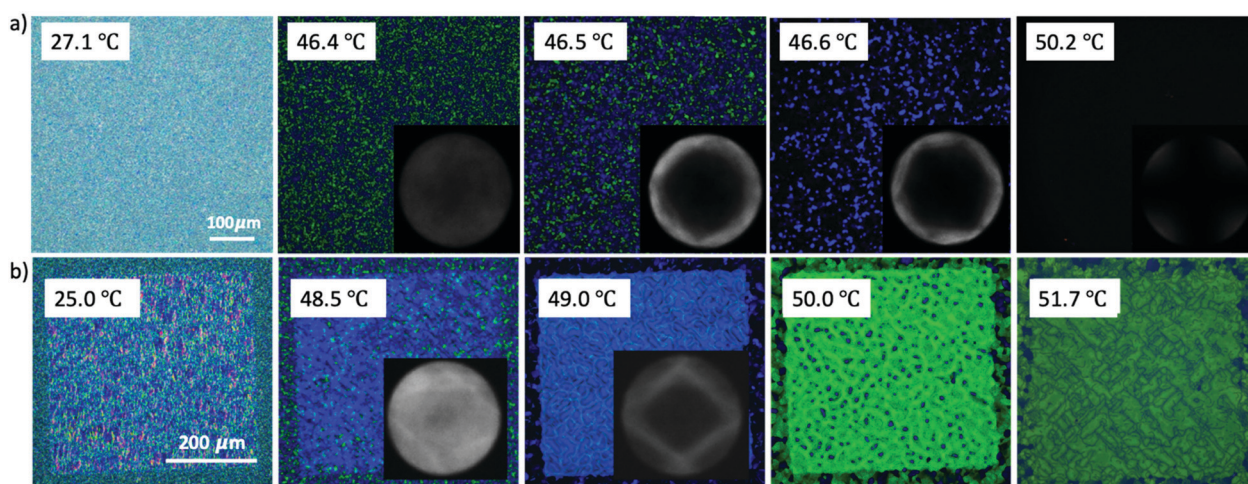
Fig. 7 Chirality Induction by the addition of chiral dopant S811 in a mixture of 13.0 wt% RM257 and BP: (a) hybrid confinement; scale bar: 100 μm; (b) directed self-assembly; scale bar: 200 μm.

increase in the lattice size. A similar transformation was observed for both planar and chemically patterned silicon substrates. The amount of chiral dopant in the system determines the chiral pitch of the cholesteric phase, which controls the size of the BP crystal lattice.[36] However, the introduction of a monomer reduces the chirality of the entire system, resulting in lattice parameter changes. The addition of the chiral dopant led to the reconstruction of BP, validating our rationale.

For BPII, the nature of the four disclination lines joined at the center of the cubic structure limits the deformation of the crystal lattice. Thus, BPII formation was prohibited beyond a certain lattice dimension and the lattice orientation (100) remained unchanged, whereas the separated disclination line structure of BPI facilitated the movement of defects and reassembly of the cubic lattice.

Reconfiguration into highly stable non-cubic morphology was confirmed by the optical characterization. The increase in the RM content led to the dynamic evolution of the BPI (110) cubic symmetry into orthorhombic, and finally reaching tetragonal (BPX). In both cases, the phase stabilization approach was similar, while the RM content differed. The presence of extra three carbons in the alkyl chains of RM82 promotes its flexibility and compatibility with the BP premixture compared to RM257. However, the addition of a non-mesogenic monomer perturbed the ordering of BPs by eliminating BPII and stabilizing BPI. After polymerization, the disclination network maintained the orthorhombic symmetry of BPI (110) and the flexibility of the condensed polymer chains widened the BP temperature range in comparison to the rigid chains.

Table 2 Variation in lattice parameters as a function of temperature for the RM82 system

RM82 (wt%)	Latttice orientation	Temperature (°C)	Lattice size (nm)	Latttice orientation	Temperature (°C)	Lattice size (nm)	Latttice orientation	Temperature (°C)	Lattice size (nm)	Latttice orientation	Temperature (°C)	Lattice size (nm)
5.6	BPI (110)	47.0	254	BPII (100)	47.3	155	BPII (100)	48.5	166	BPII (100)	49.0	166
7.6	BPI (110)	48.1	260	BPII (100)	48.3	162	BPII (100)	49.0	166	BPII (100)	50.5	170
9.6	BPI (110)	42.8	241	BPII (100)	43.5	170	BPII (100)	44.5	175	BPII (100)	45.8	179
13.0	BPI (110)	53.4	241	BPI (110)	53.6	241	BPI (110)	54.0	241	BPI (110)	55.5	247
15.0	BPI (110)	55.4	248	BPI (110)	56.0	247	BPI (110)	57.0	284	BPI (110)	57.8	285
17.0	BPI (110)	51.3	254	BPI (110)	52.0	253	BPI (110)	53.0	284	BPI (110)	54.0	285

This study provides a basis for engineering the reactive mesogen configuration for the effective thermal stabilization of BP. A tailored RM design intended for self-assembly at targeted positions will introduce additional functionalities; for instance, the modulation of PBG over the visible wavelength. Since the crystal structure affects the reflective color, the variation in lattice symmetry will tune the bandgap structure. Currently, it is controlled by the external stimuli causing residual birefringence, declined electro-optic response, and restricted bandgap shift.[34] In addition, the utilized facile approach of varying the RM type and content can modulate the PBG of BPLC. In this study, by tuning the RM parameters, the shift in wavelength from 440 nm to 600 nm was observed. The complete spectrometer data with relative intensity and wavelength variation for different monomer compositions as a function of temperature are provided in Fig. S6 and S7 (ESI†). Furthermore, the effortless access to intermediate metastable states (orthorhombic and tetragonal) for both confinements provides the potential for advanced applications since the formation of non-cubic lattice symmetries is desirable for revolutionary 3D photonic crystals.[6,37,38] The polymerized defect network of BPLC also has tremendous potential as a template for versatile applications such as the self-assembly of colloidal particles[39] and electro-optic devices.

Conclusion

In conclusion, the deformation of the BPLC cubic lattice in response to RM intrusion was tracked through optical characterization. The BP formation via the synergistic assembly of RM and LC molecules in the double-twist cylinder altered the lattice parameters. Depending on the monomer concentration, the stabilization of either BPI or BPII was observed. For the BPII (100) lattice orientation, the size of the lattice changed from 155 nm to 179 nm when the RM82 concentration was below 13.0 wt%, whereas the transition of the reflection wavelength of the BPI (110) lattice orientation was recorded from as low as 510 nm to 602 nm. RM with a rigid structure similarly affected the BP at different concentrations. The regeneration of BP after the addition of chiral dopant justified the RM assembly in DTC. Ultimately, the synergistic self-assembly of RMs in the BP lattice of the liquid crystals provides the ability to modulate the optical characteristics.

Experimental section

Materials

MLC 2142 and S-811 were purchased from Merck. RM257 and RM82 were obtained from Grandichem. Fisher Finest Premium Grade glass slides and coverslips were acquired from Fisher Scientific. Octadecyltrichlorosilane (OTS), heptane, dichloromethane (DCM), chlorobenzene, isopropyl alcohol and n-amyl acetate were purchased from MilliporeSigma and used without further purification. The LC polymer brush PMMAZO, poly (6-(4-methoxy-azobenzene-4′-oxy) hexyl methacrylate), was synthesized through a process reported by Stewart and Imrie.[40]

Preparation of PMMAZO brush chemical patterns. A PMMAZO film was deposited on a piranha-cleaned silicon substrate by spin-coating a 0.05 wt% chlorobenzene solution at 4000 rpm for 60 s and annealed at 250.0 °C for 5 min in a nitrogen atmosphere. The non-grafted PMMAZO was removed by sonication in chlorobenzene three times for 5 min, with the 3–4 nm PMMAZO brush remaining. A 40 nm-thick GL2000 photoresist film was spin-coated onto the PMMAZO brush and baked at 160.0 °C for 5 min. Patterns with an array of stripes were exposed on the resists via electron beam lithography with the JEOL 8100FS electron-beam writer at the Center for Nanoscale Materials, Argonne National Laboratory. The exposed substrates were developed in n-amyl acetate for 15 s followed by rinsing with isopropyl alcohol. The oxygen plasma etching transferred the resist pattern onto the PMMAZO brush layer. The GL2000 photoresist was further stripped by chlorobenzene through sonication.

Preparation of optical cells. The glass microscope slides were boiled in a piranha solution (7:3 (v/v) of 98% H_2SO_4/30% H_2O_2) at 130.0 °C for 1 h to remove any stains on the surface, followed by washing with DI water and drying with nitrogen. For OTS modification, the cleaned glass slides were immersed in a mixture of 13.8 μl OTS and 120 ml heptane for 1 h. Afterwards, the slides were removed from the solution and washed two times with DCM then quickly dried under a nitrogen flow. The OTS glass and a cleaned Si substrate or a Si substrate with the PMMAZO chemical pattern were placed face-to-face, with a 3.5 μm spacer, to create a cell with a hybrid anchoring or directed self-assembly approach. The optical cell and the LC were heated above the clearing point and the mixture was injected through capillary action. The system was then slowly cooled to room temperature. The UV irradiation of

13786 | *J. Mater. Chem. C*, 2022, **10**, 13778–13788

This journal is © The Royal Society of Chemistry 2022

samples with 21.2 mW cm^{-2} (measured at 365 nm) was carried out using an ultraviolet light source (Hamamatsu E11923).

Characterization. The thickness of the PMMAZO brush was measured by a Woollam VUV-VASE32 variable angle spectroscopic ellipsometer. The JEOL 8100FS electron-beam writer at the Center for Nanoscale Materials, Argonne National Laboratory was used to write chemical patterns. The optical images of the LC cell were obtained with a BX 60 Olympus polarized light microscope. The type of BP and their orientation were determined by Kossel diagrams. UV-visible spectra were recorded using a spectrophotometer (Flame UV-VIS Ocean Insight).

Author contributions

X. L. conceived and designed the experiments. T. P. and S. C. performed the experiments. X. L., T. P. and N. H. wrote the manuscript. X. L. guided the work. All authors discussed the results and contributed to data analysis and manuscript revision.

Conflicts of interest

There are no conflicts to declare.

Acknowledgements

References

1 O. D. Lavrentovich and M. Kleman, Cholesteric Liquid Crystals: Defects and Topology, In *Chirality in Liquid Crystals*, Springer New York, NY, 2001, pp. 115–158.

2 Z. Ge, S. Gauza, M. Jiao, H. Xianyu and S. Wu, Electro-optics of polymer-stabilized blue phase liquid crystal displays, *Appl. Phys. Lett.*, 2009, **94**, 101104.

3 J. Yang, J. Liu, B. G. W. He, Z. Yang, J. Wang, T. Ikeda and L. Jiang, Fabrication and photonic applications of large-domain blue phase films, *J. Mater. Chem. C*, 2019, **7**, 9460–9466.

4 C.-W. Chen, C.-T. Hou, C.-C. Li, H.-C. Jau, C.-T. Wang, C.-L. Hong, D.-Y. Guo, C.-Y. Wang, S.-P. Chiang, T. J. Bunning, I.-C. Khoo and T.-H. Lin, Large three-dimensional photonic crystals based on monocrystalline liquid crystal blue phases, *Nat. Commun.*, 2017, **8**, 727.

5 W. Cao, A. Muñoz, P. Palffy-Muhoray and B. Taheri, Lasing in a three-dimensional photonic crystal of the liquid crystal blue phase II, *Nat. Mater.*, 2002, **1**, 111–113.

6 L. Wang and Q. Li, Stimuli-Directing Self-Organized 3D Liquid-Crystalline Nanostructures: From Materials Design to Photonic Applications, *Adv. Funct. Mater.*, 2016, **26**, 10–28.

7 H. S. Kitzerow, The Effect of Electric Fields on Blue Phases, *Mol. Cryst. Liq. Cryst.*, 1991, **1991**(202), 51–83.

8 Y. Chen and S.-T. Wu, Electric field-induced monodomain blue phase liquid crystals, *Appl. Phys. Lett.*, 2013, **102**, 171110.

9 J. A. Martínez-González, X. Li, M. Sadati, Y. Zhou, R. Zhang, P. F. Nealey and J. J. de Pablo, Directed self-assembly of liquid crystalline blue-phases into ideal single-crystals, *Nat. Commun.*, 2017, **8**, 15854.

10 X. Li, J. A. Martínez-González, K. Park, C. Yu, Y. Zhou, J. J. de Pablo and P. F. Nealey, Perfection in Nucleation and Growth of Blue-Phase Single Crystals: Small Free-Energy Required to Self-Assemble at Specific Lattice Orientation, *ACS Appl. Mater. Interfaces*, 2019, **11**, 9487–9495.

11 W. Hu, L. Wang, M. Wang, T. Zhong, Q. Wang, L. Zhang, F. Chen, K. Li, Z. Miao, D. Yang and H. Yang, Ultrastable liquid crystalline blue phase from molecular synergistic self-assembly, *Nat. Commun.*, 2021, **12**, 1440.

12 H. Liu, D. Shen, X. Wang, Z. Zheng and S. Li, Wide blue phase range induced by bent-shaped molecules with acrylate end groups, *Opt. Mater. Express*, 2016, **6**, 436–443.

13 W.-Q. Yang, G.-Q. Cai, Z. Liu, X.-Q. Wang, W. Feng, Y. Feng, D. Shen and Z.-g Zheng, Room temperature stable helical blue phase enabled by a photo-polymerizable bent-shaped material, *J. Mater. Chem. C*, 2017, **5**, 690–696.

14 M. Wang, W. Hu, L. Wang, D.-Y. Guo, T.-H. Lin, L. Zhang and H. Yang, Reversible light-directed self-organized 3D liquid crystalline photonic nanostructures doped with azobenzene-functionalized bent-shaped molecules, *J. Mater. Chem. C*, 2018, **6**, 7740–7744.

15 J. Wang, Y. Shi, K. Yang, J. Wei and J. Guo, Stabilization and optical switching of liquid crystal blue phase doped with azobenzene-based bent-shaped hydrogen-bonded assemblies, *RSC Adv.*, 2015, **5**, 67357–67364.

16 H. Li, W. Huang, Q. Mo, B. Liu, D. Shen, W. Zhang and Z.-g Zheng, Stable soft cubic superstructure enabled by hydrogen-bond complex functionalized polymer/liquid crystal system, *J. Mater. Chem. C*, 2019, **7**, 3952–3957.

17 Y. Shi, X. Wang, J. Wei, H. Yang and J. Guo, Stabilization of blue phases by hydrogen-bonded bent-shaped and T-shaped molecules featuring a branched terminal group, *Soft Matter*, 2013, **9**, 10186.

18 H. Li, W. Huang, Q. Mo, B. Liu, D. Shen, W. Zhang and Z.-g Zheng, Stable soft cubic superstructure enabled by hydrogen-bond complex functionalized polymer/liquid crystal system, *J. Mater. Chem. C*, 2019, **7**, 3952–3957.

19 K.-W. Park, M.-J. Gim, S. Kim, S.-T. Hur and S.-W. Choi, Liquid-crystalline blue phase II system comprising a bent-core molecule with a wide stable temperature Range, *ACS Appl. Mater. Interfaces*, 2013, **5**(16), 8025–8029.

20 H. Yoshida, Y. Tanaka, K. Kawamoto, H. Kubo, T. Tsuda, A. Fujii, S. Kuwabata, H. Kikuchi and M. Ozaki,

This journal is © The Royal Society of Chemistry 2022

J. Mater. Chem. C, 2022, **10**, 13778–13788 | **13787**

Nanoparticle-Stabilized Cholesteric Blue Phases, *Appl. Phys. Express*, 2009, **2**, 121501.

21 L. Wang, W. He, Q. Wang, M. Yu, X. Xiao, Y. Zhang, M. Ellahi, D. Zhao, H. Yang and L. Guo, Polymer-stabilized nanoparticle-enriched blue phase liquid crystals, *J. Mater. Chem. C*, 2013, **1**, 6526.

22 N. Kasch, I. Dierking and M. Turner, Stabilization of the liquid crystalline blue phase by the addition of short-chain polystyrene, *Soft Matter*, 2013, **9**, 4789–4793.

23 H. Kikuchi, M. Yokota, Y. Hisakado, H. Yang and T. Kajiyama, Polymer-stabilized liquid crystal blue phases, *Nat. Mater.*, 2002, **1**, 64–68.

24 H. Kikuchi, S. Izena, H. Higuchi, Y. Okumura and H. Higashiguchi, Giant Polymer Lattice in a Polymer-stabilized Blue Phase Liquid Crystal, *Soft Matter*, 2015, **11**, 4572–4575.

25 E. Kemiklioglu, The effects of the long flexible chain reactive monomers on blue phase liquid crystals, *Polymer*, 2018, **148**, 278–283.

26 J. Yang, W. Zhao, Z. Yang, W. He, J. Wang, T. Ikeda and L. Jiang, Photonic Shape Memory Polymer Based on Liquid Crystalline Blue Phase Films, *ACS Appl. Mater. Interfaces*, 2019, **11**, 46124–46131.

27 R. Manda, S. Pagidi, Y. Heo, Y. J. Lim, M. Kim and S. H. Lee, Electrically tunable photonic band gap structure in monodomain blue-phase liquid crystals, *NPG Asia Mater.*, 2020, **12**, 42.

28 Y.-S. Zhang, S.-A. Jiang, J.-D. Lin, P.-C. Yang and C.-R. Lee, Stretchable Freestanding Films of 3D Nanocrystalline Blue Phase Elastomer and Their Tunable Applications, *Adv. Opt. Mater.*, 2021, **9**, 2001427.

29 F. Castles, S. M. Morris, J. M. C. Hung, M. M. Qasim, A. D. Wright, S. Nosheen, S. S. Choi, B. I. Outram, S. J. Elston, C. Burgess, L. Hill, T. D. Wilkinson and H. J. Coles, Stretchable liquid-crystal blue-phase gels, *Nat. Mater.*, 2014, **13**, 817–821.

30 I. Chiang, C. Long, H. Lin, W. Chuang, J. Lee and H. Lin, Broad Ranges and Fast Responses of Single-Component Blue-Phase Liquid Crystals Containing Banana-Shaped 1,3,4-Oxadiazole Cores, *ACS Appl. Mater. Interfaces*, 2014, **6**, 228–235.

31 A. Hauser, M. Thieme, A. Saupe, G. Heppke and D. Krüerke, Surface-imaging of frozen blue phases in a discotic liquid crystal with atomic force microscopy, *J. Mater. Chem.*, 1997, **7**, 2223–2229.

32 P. Cladis, T. Garel and P. Pieranski, Kossel diagrams show electric-field-induced cubic-tetragonal structural transition in frustrated liquid-crystal blue phases, *Phys. Rev. Lett.*, 1986, **57**, 2841–2844.

33 S. Cho, M. Takahashi, J. Fukuda, H. Yoshida and M. Ozaki, Directed self-assembly of soft 3D photonic crystals for holograms with omnidirectional circular-polarization selectivity, *Commun. Mater.*, 2021, **2**, 1–9.

34 D. Guo, C. Chen, C. Li, H. Jau, K. Lin, T. Feng, C. Wang, T. J. Bunning, I. C. Khoo and T. Lin, Reconfiguration of three-dimensional liquid-crystalline photonic crystals by electrostriction, *Nat. Mater.*, 2020, **19**, 94–101.

35 Y. Zhang, H. Yoshida, S. Cho, J. Fukuda and M. Ozaki, In Situ Optical Characterization of Twinning in Liquid Crystalline Blue Phases, *ACS Appl. Mater. Interfaces*, 2021, **13**, 36130–36137.

36 E. Otón, H. Yoshida, P. Morawiak, O. Strzeżysz, P. Kula, M. Ozaki and W. Piecek, Orientation control of ideal blue phase photonic crystals, *Sci. Rep.*, 2020, **10**, 10148.

37 Y. Yang, L. Wang, H. Yang and Q. Li, 3D Chiral Photonic Nanostructures Based on Blue-Phase Liquid Crystals, *Small Sci.*, 2021, **1**, 2100007.

38 H. K. Bisoyi and Q. Li, Liquid Crystals: Versatile Self-Organized Smart Soft Materials, *Chem. Rev.*, 2022, **122**, 4887–4926.

39 S. Žumer, N. A. Clark, G. P. Alexander, J. M. Yeomans and M. Ravnik, Three-dimensional colloidal crystals in liquid crystalline blue phases, *Proc. Natl. Acad. Sci. U. S. A.*, 2011, **108**, 5188–5192.

40 D. Stewart and C. T. Imrie, Synthesis and characterization of spin-labelled and spin-probed side-chain liquid crystal polymers, *Polymer*, 1996, **37**, 3419–3425.

13788 | *J. Mater. Chem. C*, 2022, **10**, 13778–13788

This journal is © The Royal Society of Chemistry 2022